

# Direct Evidence of the Benzylium and Tropylium Cations as the two long-lived Isomers of $C_7H_7^+$

Pavol Jusko,<sup>[a]</sup> Aude Simon,<sup>[b]</sup> Shreyak Banhatti,<sup>[c]</sup> Sandra Brünken,<sup>[d]</sup>  
Christine Joblin<sup>[a],\*</sup>

Submitted version. Final version in Chem. Phys. Chem.;

<http://dx.doi.org/10.1002/cphc.201800744>

## Abstract

Disentangling the isomeric structure of  $C_7H_7^+$  is a longstanding experimental issue. We report here the full mid-infrared vibrational spectrum of  $C_7H_7^+$  tagged with Ne obtained with infrared-predissociation spectroscopy at 10 K. Saturation depletion measurements were used to assign the contribution of benzylium and tropylium isomers and demonstrate that no other isomer is involved. Recorded spectral features compare well with density functional theory calculations. This opens perspectives for a better understanding and control of the formation paths leading to either tropylium or benzylium ions.

Benzylium ( $Bz^+$ ) and tropylium ( $Tr^+$ ) ions are key isomers of  $C_7H_7^+$  commonly produced from energized toluene ( $C_7H_8$ ).<sup>[1,2,3]</sup> Whereas  $Bz^+$  consists of a benzene ring substituted with a methylene group, the  $Tr^+$  isomer is a fully aromatic ion made of a 7-membered CH ring. The possibility that similar structures can be involved in the fragmentation of methyl-substituted polycyclic aromatic hydrocarbon ions has been recently discussed.<sup>[4,5]</sup> Still, one of the major issues in these studies is the limited understanding of the formation paths of these species, that would allow us to predict and therefore control the production of one or the other isomer. On the one hand, it was shown that the choice of the precursor is important, e.g., the use of halogen-substituted toluene is expected to optimise the production of  $Bz^+$ .<sup>[6]</sup> But on the other hand, the  $Bz^+/Tr^+$  ratio depends strongly on the various experimental conditions.<sup>[7,8]</sup> Another point, in photoionization experiments of toluene, is that it is not possible to produce solely  $Tr^+$  at appearance threshold,<sup>[9]</sup> despite calculations show  $Tr^+$  being energetically more favorable than  $Bz^+$  (by  $\sim 38 \text{ kJ} \cdot \text{mol}^{-1}$ ; cf. Tab S3 in the SI). The latter results were interpreted as due both to the presence of a barrier in the dissociation path from toluene towards  $Tr^+$ , and to the role of autoionizing states in promoting a nonstatistical formation of  $Bz^+$  over  $Tr^+$ .<sup>[9]</sup> In contrast to  $Tr^+$ , theoretical studies show that paths towards  $Bz^+$  lack high barriers, and no barrier is found in the path from benzyl chloride ionization towards  $Bz^+$  formation.<sup>[10]</sup>

It is known since earlier studies on  $C_7H_7^+$  that a convenient way to identify  $Bz^+$  is through ion-molecule reaction with toluene, leading to efficient formation of  $C_8H_9^+$ .<sup>[11,1]</sup> The non-reactive part of the ion population is then attributed to  $Tr^+$ . In parallel, there have been many attempts to characterize the structure of  $C_7H_7^+$  directly, i.e., via spectroscopy. Electronic absorption features have been studied in both Ne matrix<sup>[12]</sup> and in gas-phase by photodissociation.<sup>[13,14]</sup> For  $Bz^+$ , the vibronic structure was resolved for the  $S_1 \leftarrow S_0$  transition but much broader features were observed for the higher excited states. Absorption features of  $Tr^+$  are expected in the UV range,<sup>[12]</sup> but the

<sup>[a]</sup> Institut de Recherche en Astrophysique et Planétologie (IRAP), Université de Toulouse (UPS), CNRS, CNES, 9 Av. du Colonel Roche, 31028 Toulouse Cedex 4, France.

<sup>[b]</sup> Laboratoire de Chimie et Physique Quantiques LCPQ/IRSAMC, Université de Toulouse (UPS) and CNRS, 118 Route de Narbonne, 31062 Toulouse, France.

<sup>[c]</sup> I. Physikalisches Institut, Universität zu Köln, Zùlpicher Str. 77, 50937 Köln, Germany.

<sup>[d]</sup> Radboud University, Institute for Molecules and Materials, FELIX Laboratory, Toernooiveld 7c, 6525 ED, Nijmegen, The Netherlands.

\* christine.joblin@irap.omp.eu

data obtained in Ne matrices could not be confirmed in the gas-phase.<sup>[13]</sup> On the opposite, infrared and Raman spectra of  $\text{Tr}^+$  could be obtained in solutions or in solid phase using salts.<sup>[15,16,17]</sup> In gas-phase, one can think of infrared multiple photon dissociation (IRMPD) vibrational spectroscopy as the technique of choice when characterizing the structure of ions in mass spectrometry experiments.<sup>[18]</sup> Information on the  $\text{Bz}^+/\text{Tr}^+$  dichotomy<sup>[19]</sup> could be obtained from the IRMPD spectra of derivative ions with lower dissociation thresholds compared to  $\text{C}_7\text{H}_7^+$ .<sup>[20,21,19,22]</sup> The spectroscopy of polycyclic hydrocarbon cations containing  $\text{Bz}^+$  and  $\text{Tr}^+$  structure was also investigated.<sup>[8,5]</sup> However, the IRMPD spectra of pure  $\text{Bz}^+$  and  $\text{Tr}^+$  are still lacking, despite the efforts.<sup>[20]</sup> This could be due to the exceptional stability of these ions, or possible isomerisation issues, as found in the case of  $\text{C}_{17}\text{H}_{11}^+$ .<sup>[5]</sup>

An alternative approach to IRMPD not owning the disadvantages of the multi-photon process, is infrared pre-dissociation (IR-PD) spectroscopy of a weakly bound complex of the ion with a rare gas atom. Thanks to this technique, we were able to obtain the first complete mid-IR-PD spectra of Ne tagged  $\text{C}_7\text{H}_7^+$  recorded in gas-phase and at low temperature. We used the cryogenic 22 pole ion trap,<sup>[23]</sup> which is coupled to the free electron laser FELIX, as described in the experimental section below. We introduced different precursors and varied the ionization conditions (cf. Tab. S1 in the SI). Figure 1 gathers the recorded experimental spectra, which appear to agree well with the calculated spectra of  $\text{Bz}^+$  and  $\text{Tr}^+$  using density functional theory (DFT) at the B3LYP/6-31G(d,p) level of theory as implemented in Gaussian09 suite of programs.<sup>[24]</sup> In addition, the contribution of  $\text{Bz}^+$  and  $\text{Tr}^+$  in each mixture could be determined directly during the spectroscopic experiment by using saturation depletion measurements. To achieve the latter, the laser is tuned in resonance with a vibrational band of interest. By applying a large number of photon pulses, the optically active isomer-Ne complex can be dissociated completely leaving only the optically inactive isomer-Ne complex in the trap. Recording the ion-Ne ( $m = 111\text{ u}$ ) number as a function of time reveals the relative abundance of active to inactive isomers. Depletion tests for selected bands of both isomers and under varying ion source conditions are shown in Fig. 2. They show that one condition leads to 90%  $\text{Bz}^+$  population and another to 60-70% of  $\text{Tr}^+$  with 40-30% of  $\text{Bz}^+$ . These measurements provide the first complete demonstration that  $\text{Bz}^+$  and  $\text{Tr}^+$  are the only long-lived isomers of  $\text{C}_7\text{H}_7^+$ . In a preparatory study, we also recorded the chemical reactivity with toluene and found a good agreement with the above measurements, although only  $\text{Bz}^+$  can be directly monitored (cf. Fig. S2 in the SI).

Assignment of the experimental bands of  $\text{Bz}^+$  and  $\text{Tr}^+$  is made in Tables 1 and 2. Additional levels of theory were carried out for benchmarking (cf. Section 2 in the SI). For each level, the calculated band positions are linearly scaled with a scaling factor  $S$ , in order to match with the strongest  $\text{Bz}^+$  band. From calculations on Ne tagged ions, we found that the top (T) and molecular plane (P) isomers are quasi degenerate (cf. Tab. S3 in the SI) and that the Ne tag is not expected to induce band shifts (cf. Figs. S12 and S13, Table S4 in the SI), nor splitting of the bands due to the degeneracy lifting in the  $\text{Tr}^+$  case, that would be observable in our experiments (cf. Fig. S12 in the SI, degenerate bands always split by less than  $1\text{ cm}^{-1}$ ). Overall, we found a good agreement between the measured and calculated band positions. However, in the case of  $\text{Tr}^+$ , one major difference exists. The harmonic calculations provide only three infrared active bands, which can be rationalized by the high symmetry of  $\text{Tr}^+$  which pertains to the  $\text{D}_{7h}$  point group symmetry (cf. Tab. S2 in the SI for descent in symmetry from  $\text{D}_{7h}$  to  $\text{C}_{2v}$ , in which calculations are performed). In the experimental spectrum, we found four bands, two bands including the additional one falling at low frequency. We note that two close-by bands in this range are also observed in some experiments in condensed phase.<sup>[15,16,17]</sup>

Saturation depletion measurements established that bands (b) – (d) in the experimental spectrum (Fig. 1), belong solely to  $\text{Tr}^+$ , and that both  $\text{Bz}^+$  and  $\text{Tr}^+$  are active at the  $630\text{ cm}^{-1}$  band (a). Bands (c) and (d) can be assigned to the doubly degenerate in plane CH bending mode and in plane CC stretching mode of  $\text{Tr}^+$ , respectively. The third  $\text{Tr}^+$  band, the CH out-of-plane bending

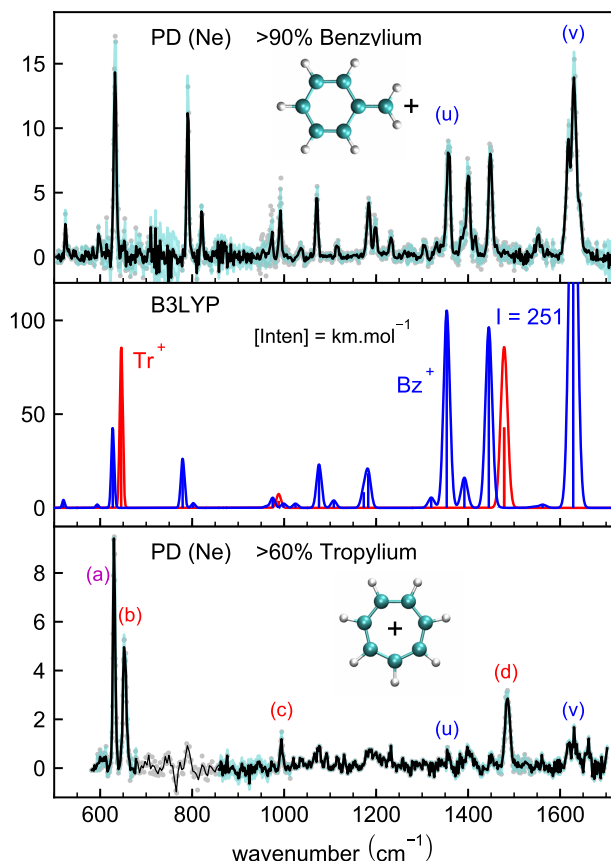


Figure 1: Mid-IR spectrum of  $C_7H_7^+$ . Top panel – IR pre-dissociation spectrum of  $Bz^+$  tagged with Ne. Middle panel – stick spectrum corresponding to the scaled DFT harmonic spectra for  $Bz^+$  (blue) and  $Tr^+$  (red). Convolved spectra with  $\sigma = 0.5\%$  BW are provided for comparison with the experiment. Bottom panel – IR pre-dissociation spectrum of  $Tr^+$  tagged with Ne. Bands marked by (a), (b), (c), (d) have been confirmed to belong to  $Tr^+$  and those marked (a), (u), (v) to  $Bz^+$  by saturation depletion measurements. Intensities for experimental spectra are in arbitrary units. All recorded bands are listed in Tab. 1 for  $Bz^+$  and Tab. 2 for  $Tr^+$ .

mode (not degenerate) should lay around  $650\text{ cm}^{-1}$  (close to band (b), cf. Fig. S3). The performed saturation depletion measurements invalidate the hypothesis that both bands (a) and (b) are caused by distinct (T) and (P)  $Tr^+ \cdot Ne$  isomers. We also excluded contribution from a triplet spin state, whose presence can lead to shifts in low energy modes for PAHs.<sup>[25]</sup> In the case of  $Tr^+$ , it was found distorted and 3.3 eV above the ground state at the B3LYP/6-31G(d,p) level of theory (cf. Fig. S14 in the SI for its computed IR spectrum). The excited state can not survive many collisions with cold buffer gas and its spectrum does not contain features in the wavelength range of interest. The most likely scenario to account for bands (a) and (b), is that a combination band comes into close resonance with the fundamental CH out-of-plane bending mode, and borrows a significant part of its intensity. Our calculations show that the combination band involves the two lowest vibrational modes of  $Tr^+$  and that the combination band is red shifted relative to the fundamental band (Tab. 2 and Tab. S5 in the SI). In our experiment, we can assign band (b) as the fundamental mode (i.e. the strongest band) since the initial dissociation rate of this band is higher and its band width at saturation is larger as compared to band (a) (Fig. 2). Finally, our spectra do not include the CH stretch range. However, we learned while writing this manuscript that this range has recently been studied using a jet experiment and a table-top laser.<sup>[26]</sup>

We recorded the mid-IR-PD spectra of  $C_7H_7^+$  tagged with Ne at 10 K. The comparison of

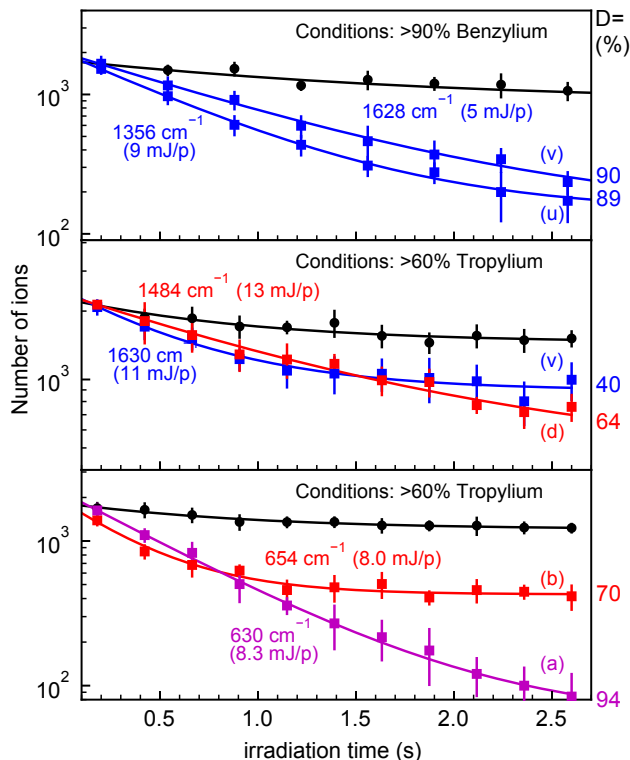


Figure 2: Depletion of  $C_7H_7^+ \cdot Ne$  in the ion trap for the different experimental conditions used in Fig.1. Color code: Blue – wavelength at which the  $Bz^+$  isomer is active. Red – wavelength at which the  $Tr^+$  isomer is active. Magenta – both isomers active. Black – corresponds to non-resonant dissociation of the Ne tag ( $\sim 8 - 10$  mJ/pulse). Numbers in the right column correspond to saturation depletion in percent. Letters refer to the bands shown in Fig. 1.

the experimental spectra with the harmonic calculated spectra show, that neither significant band shifts, nor band splitting are induced by the presence of the Ne tag, that can in particular induce a symmetry decrease in the case of  $Tr^+$ . The  $Tr^+$  spectrum exhibits an interesting strong resonance at low frequency between a combination band and the fundamental CH out-of-plane bending mode. Anharmonic calculations would help in providing a detailed quantitative study of this resonance.<sup>[27,28]</sup>

We used saturation depletion measurements to confirm the existence of only two long-lived isomers of  $C_7H_7^+$ , and the obtained spectra support their initial structural assumption as  $Bz^+$  and  $Tr^+$ .<sup>[1,9]</sup> The depletion technique in an ion trap has the advantage of being able to track the abundance of a well-defined isomer, contrary to the earlier reactivity method, which only has access to  $Bz^+$ . This technique opens new perspectives for our understanding of the isomerisation paths of  $C_7H_7^+$ .

## Experimental Section

The ions are produced by electron bombardment in a storage type ion source<sup>[29]</sup> from benzyl chloride and toluene precursors. Ions of mass 91  $u$  ( $C_7H_7^+$ ) are mass selected in a quadrupole mass filter prior to being injected into the cryogenic 22 pole rf ion trap (nominal temperature 8 – 9 K), where they are cooled by a 100 ms long 3:1 He:Ne gas pulse. The high number gas density achieved during this pulse ( $n \sim 10^{14} \text{ cm}^{-3}$ ) promotes ternary attachment of Ne to the bare ion producing  $Bz^+ \cdot Ne$  and  $Tr^+ \cdot Ne$  complexes. After the cooling and tagging sequence, the number density in the trap

Table 1: Experimental mid-IR band positions recorded for  $\text{Bz}^+$  and calculated values using DFT (B3LYP/6-31G(d,p)) obtained in the present work (see Figure 1). Only the modes which are IR active are reported. Their symmetry in the point group of the molecular ion ( $\text{C}_{2v}$ ) are reported.

Mode	Exp.		Calc.	
	$\nu$	$\nu$	Inten.	Sym.
$\nu_5$	524	521	4.3	$\text{A}_1$
$\nu_6$	596	594	1.8	$\text{B}_2$
$\nu_8$	632	628	42.8	$\text{B}_1$
$\nu_9$	790	780	26.3	$\text{B}_1$
$\nu_{10}$	820	803	2.6	$\text{A}_1$
$\nu_{12}$		962	0.9	$\text{B}_2$
$\nu_{13}$	974	976	5.4	$\text{A}_1$
$\nu_{16}$	992	1000	2.4	$\text{A}_1$
$\nu_{17}$	1036	1026	2.3	$\text{B}_1$
$\nu_{18}$	1070	1077	23.2	$\text{B}_1$
$\nu_{19}$	1114	1109	4.0	$\text{B}_2$
$\nu_{20}$	1184	1174	8.4	$\text{B}_2$
$\nu_{21}$	1198	1184	18.5	$\text{A}_1$
	1232			
	1302			
$\nu_{22}$	1332	1321	5.6	$\text{B}_2$
$\nu_{23}$	1356	1355	105.5	$\text{A}_1$
$\nu_{24}$	1400	1393	16.1	$\text{B}_2$
$\nu_{25}$	1448	1446	96.4	$\text{B}_2$
$\nu_{26}$		1467	0.2	$\text{A}_1$
$\nu_{27}$		1541	0.6	$\text{B}_2$
$\nu_{28}$	1554	1564	1.8	$\text{A}_1$
$\nu_{29}^*$	1630	1630	250.9	$\text{A}_1$

*Note:* All frequencies in  $\text{cm}^{-1}$ , intensities in  $\text{km} \cdot \text{mol}^{-1}$ . \* – mode used to determine the scaling factor 0.974. Cf. Fig. S15. in the SI for the visualisation of modes.

Table 2: Experimental mid-IR band positions recorded for  $\text{Tr}^+$  and calculated values using DFT (B3LYP/6-31G(d,p)) obtained in the present work (see Figure 1). Only the modes which are IR active are reported. Although they were computed in the  $\text{C}_{2v}$  symmetry point group, their symmetry in the point group of the molecular ion ( $\text{D}_{7h}$ ) are listed.

Mode	Exp.		Ref.		Calc.	
	$\nu$		$\nu$		$\nu$ (Inten.)	Sym.
$\nu_c$	630	633, <sup>[15]</sup>	634, <sup>[16]</sup>	655 <sup>[17]</sup>		
$\nu_4$	652	658, <sup>[15]</sup>	660, <sup>[16]</sup>	685 <sup>[17]</sup>	646(85.8)	$\text{A}''_2$
$\nu_8$	994	992, <sup>[15]</sup>	992 <sup>[16]</sup>		989(3.7)	$\text{E}'_1$
$\nu_{14}$	1486	1477, <sup>[15]</sup>	1477 <sup>[16]</sup>		1480(42.9)	$\text{E}'_1$

*Note:* All frequencies in  $\text{cm}^{-1}$ , intensities in  $\text{km} \cdot \text{mol}^{-1}$ . Scaling factor 0.974.  $\nu_c$  is a combination band of the two lowest lying fundamental bands of  $\text{Tr}^+$ . Cf. Fig. S16 – S18. in the SI for the visualisation of modes.

decreases quickly to a level where no further attachment takes place. The ion–Ne complex is then dissociated by infrared radiation provided by the FELIX FEL-2 free electron laser,<sup>[30]</sup> operated in the 500 – 1650 cm<sup>-1</sup> range. The laser delivers up to 30 mJ in a single macropulse into the 22 pole trap with a repetition rate of 10 Hz and spectral bandwidth better than  $\sigma = 0.5\%$ . After an irradiation time of typically 2.6 s the trap content is emptied through a mass filter onto a counting detector.

## Acknowledgements

The research leading to this result is supported by the European Research Council under the European Union’s Seventh Framework Programme ERC-2013-SyG, Grant Agreement n. 610256 NANOCOSMOS. We acknowledge support from the project CALIPSOplus under the Grant Agreement 730872 from the EU Framework Programme for Research and Innovation HORIZON 2020. We greatly appreciate the experimental support provided by the FELIX team. We gratefully acknowledge the Nederlandse Organisatie voor Wetenschappelijk Onderzoek (NWO) for the support of the FELIX Laboratory. We thank the Cologne Laboratory Astrophysics group for providing the FELion ion trap instrument and the Cologne Center for Terahertz Spectroscopy (core facility, DFG grant SCHL 341/15-1) for supporting its operation. S.Ba. is supported by the H2020-MSCA-ITN-2016 Program (EUROPAH project, G. A. 722346). A. S. thanks the computing facility CALMIP for generous allocation of computer resources.

**Keywords:** benzylium; tropylium; structure elucidation; IR spectroscopy; cryogenic ion trap

## References

- [1] R. C. Dunbar, *Journal of the American Chemical Society* **1975**, *97*, 1382–1384, DOI [10.1021/ja00839a016](https://doi.org/10.1021/ja00839a016).
- [2] D. Kuck, *Mass Spectrometry Reviews* **1990**, *9*, 583–630, DOI [10.1002/mas.1280090602](https://doi.org/10.1002/mas.1280090602).
- [3] C. Lifshitz, *Accounts of Chemical Research* **1994**, *27*, 138–144, DOI [10.1021/ar00041a004](https://doi.org/10.1021/ar00041a004).
- [4] M. Rapacioli, A. Simon, C. C. M. Marshall, J. Cuny, D. Kokkin, F. Spiegelman, C. Joblin, *The Journal of Physical Chemistry A* **2015**, *119*, 12845–12854, DOI [10.1021/acs.jpca.5b09494](https://doi.org/10.1021/acs.jpca.5b09494).
- [5] P. Jusko, A. Simon, G. Wenzel, S. Brünken, S. Schlemmer, C. Joblin, *Chemical Physics Letters* **2018**, *698*, 206 – 210, DOI [10.1016/j.cplett.2018.03.028](https://doi.org/10.1016/j.cplett.2018.03.028).
- [6] J. A. A. Jackson, S. G. Lias, P. Ausloos, *Journal of the American Chemical Society* **1977**, *99*, 7515–7521, DOI [10.1021/ja00465a020](https://doi.org/10.1021/ja00465a020).
- [7] T. D. Fridgen, J. Troe, A. A. Viggiano, A. J. Midey, S. Williams, T. B. McMahon, *The Journal of Physical Chemistry A* **2004**, *108*, 5600–5609, DOI [10.1021/jp031328s](https://doi.org/10.1021/jp031328s).
- [8] D. Morsa, V. Gabelica, F. Rosu, J. Oomens, E. De Pauw, *The Journal of Physical Chemistry Letters* **2014**, *5*, 3787–3791, DOI [10.1021/jz501903b](https://doi.org/10.1021/jz501903b).
- [9] C. Lifshitz, Y. Gotkis, J. Laskin, A. Ioffe, S. Shaik, *The Journal of Physical Chemistry* **1993**, *97*, 12291–12295, DOI [10.1021/j100149a032](https://doi.org/10.1021/j100149a032).
- [10] J. C. Choe, *The Journal of Physical Chemistry A* **2008**, *112*, 6190–6197, DOI [10.1021/jp802641c](https://doi.org/10.1021/jp802641c).

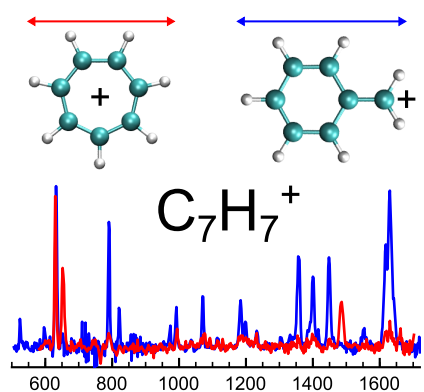


- [11] J. Shen, R. C. Dunbar, G. A. Olah, *Journal of the American Chemical Society* **1974**, *96*, 6227–6229, DOI [10.1021/ja00826a070](https://doi.org/10.1021/ja00826a070).
- [12] A. Nagy, J. Fulara, I. Garkusha, J. P. Maier, *Angewandte Chemie International Edition* **2011**, *50*, 3022–3025, DOI [10.1002/anie.201008036](https://doi.org/10.1002/anie.201008036).
- [13] V. Dryza, N. Chalyavi, J. A. Sanelli, E. J. Bieske, *The Journal of Chemical Physics* **2012**, *137*, 204304, DOI [10.1063/1.4767402](https://doi.org/10.1063/1.4767402).
- [14] G. Féraud, C. Dedonder-Lardeux, S. Soorkia, C. Jouvet, *The Journal of Chemical Physics* **2014**, *140*, 024302, DOI [10.1063/1.4858409](https://doi.org/10.1063/1.4858409).
- [15] W. G. Fateley, E. R. Lippincott, *The Journal of Chemical Physics* **1957**, *26*, 1471–1481, DOI [10.1063/1.1743566](https://doi.org/10.1063/1.1743566).
- [16] C. Sourisseau, *Spectrochimica Acta Part A: Molecular Spectroscopy* **1978**, *34*, 881 – 887, DOI [10.1016/0584-8539\(78\)80007-5](https://doi.org/10.1016/0584-8539(78)80007-5).
- [17] J. Howard, D. Graham, *Spectrochimica Acta Part A: Molecular Spectroscopy* **1985**, *41*, 815 – 824, DOI [10.1016/0584-8539\(85\)80027-1](https://doi.org/10.1016/0584-8539(85)80027-1).
- [18] J. Oomens, B. G. Sartakov, G. Meijer, G. von Helden, *International Journal of Mass Spectrometry* **2006**, *254*, 1–19, DOI [10.1016/j.ijms.2006.05.009](https://doi.org/10.1016/j.ijms.2006.05.009).
- [19] B. Chiavarino, M. E. Crestoni, O. Dopfer, P. Maître, S. Fornarini, *Angewandte Chemie International Edition* **2012**, *51*, 4947–4949, DOI [10.1002/anie.201200558](https://doi.org/10.1002/anie.201200558).
- [20] B. Chiavarino, M. E. Crestoni, S. Fornarini, O. Dopfer, J. Lemaire, P. Maître, *The Journal of Physical Chemistry A* **2006**, *110*, 9352–9360, DOI [10.1021/jp0628380](https://doi.org/10.1021/jp0628380).
- [21] D. Schröder, H. Schwarz, P. Milko, J. Roithová, *The Journal of Physical Chemistry A* **2006**, *110*, 8346–8353, DOI [10.1021/jp056962f](https://doi.org/10.1021/jp056962f).
- [22] E.-L. Zins, C. Pepe, D. Schröder, *Faraday Discuss.* **2010**, *145*, 157–169, DOI [10.1039/B907236E](https://doi.org/10.1039/B907236E).
- [23] O. Asvany, F. Bielau, D. Moratschke, J. Krause, S. Schlemmer, *Review of Scientific Instruments* **2010**, *81*, 076102, DOI [10.1063/1.3460265](https://doi.org/10.1063/1.3460265).
- [24] M. J. Frisch, G. W. Trucks, H. B. Schlegel, G. E. Scuseria, M. A. Robb, J. R. Cheeseman, G. Scalmani, V. Barone, B. Mennucci, G. A. Petersson, H. Nakatsuji, M. Caricato, X. Li, H. P. Hratchian, A. F. Izmaylov, J. Bloino, G. Zheng, J. L. Sonnenberg, M. Hada, M. Ehara, K. Toyota, R. Fukuda, J. Hasegawa, M. Ishida, T. Nakajima, Y. Honda, O. Kitao, H. Nakai, T. Vreven, J. A. Montgomery, Jr., J. E. Peralta, F. Ogliaro, M. Bearpark, J. J. Heyd, E. Brothers, K. N. Kudin, V. N. Staroverov, R. Kobayashi, J. Normand, K. Raghavachari, A. Rendell, J. C. Burant, S. S. Iyengar, J. Tomasi, M. Cossi, N. Rega, J. M. Millam, M. Klene, J. E. Knox, J. B. Cross, V. Bakken, C. Adamo, J. Jaramillo, R. Gomperts, R. E. Stratmann, O. Yazyev, A. J. Austin, R. Cammi, C. Pomelli, J. W. Ochterski, R. L. Martin, K. Morokuma, V. G. Zakrzewski, G. A. Voth, P. Salvador, J. J. Dannenberg, S. Dapprich, A. D. Daniels, Ö. Farkas, J. B. Foresman, J. V. Ortiz, J. Cioslowski, D. J. Fox, *Gaussian 09, Revision D.01*, Gaussian Inc., Wallingford CT, 2016.
- [25] C. Falvo, F. Calvo, P. Parneix, *The Journal of Chemical Physics* **2012**, *137*, 064303, DOI [10.1063/1.4739468](https://doi.org/10.1063/1.4739468).

- [26] J. P. Wagner, D. C. McDonald, M. A. Duncan, *The Journal of Physical Chemistry Letters* **2018**, *9*, 4591–4595, DOI [10.1021/acs.jpcllett.8b02121](https://doi.org/10.1021/acs.jpcllett.8b02121).
- [27] C. J. Mackie, A. Candian, X. Huang, E. Maltseva, A. Petignani, J. Oomens, W. J. Buma, T. J. Lee, A. G. G. M. Tielens, *The Journal of Chemical Physics* **2015**, *143*, 224314, DOI [10.1063/1.4936779](https://doi.org/10.1063/1.4936779).
- [28] G. Mulas, C. Falvo, P. Cassam-Chenaï, C. Joblin, *accepted in J. Chem. Phys.* **2018**, DOI <http://arxiv.org/abs/1809.05669>.
- [29] D. Gerlich in *Adv. Chem. Phys.: State-Selected and State-to-State Ion-Molecule Reaction Dynamics, Vol. LXXXII* (Eds.: C.-Y. Ng, M. Baer), Wiley, New York, **1992**, pp. 1–176, DOI [10.1002/9780470141397.ch1](https://doi.org/10.1002/9780470141397.ch1).
- [30] D. Oepts, A. F. G. van der Meer, P. W. van Amersfoort, *Infrared Physics and Technology* **1995**, *36*, 297–308, DOI [10.1016/1350-4495\(94\)00074-U](https://doi.org/10.1016/1350-4495(94)00074-U).



## Entry for the Table of Contents



**$\text{C}_7\text{H}_7^+$  isomers:** by using infrared pre-dissociation spectroscopy and saturation depletion measurements of  $\text{C}_7\text{H}_7^+ \cdot \text{Ne}$  complexes, we demonstrate that benzylium and tropylium cations are the only two long-lived isomers of gas-phase  $\text{C}_7\text{H}_7^+$ .

## Supplementary Information

### Direct Evidence of the Benzylium and Tropylium Cations as the two long-lived Isomers of $\text{C}_7\text{H}_7^+$

*Pavol Jusko,<sup>[a]</sup> Aude Simon,<sup>[b]</sup> Shreyak Banhatti,<sup>[c]</sup> Sandra Brünken,<sup>[d]</sup> Christine Joblin<sup>[a],\*</sup>*

July 31, 2018

---

<sup>[a]</sup> Institut de Recherche en Astrophysique et Planétologie (IRAP), Université de Toulouse (UPS), CNRS, CNES, 9 Av. du Colonel Roche, 31028 Toulouse Cedex 4, France.

<sup>[b]</sup> Laboratoire de Chimie et Physique Quantiques LCPQ/IRSAMC, Université de Toulouse (UPS) and CNRS, 118 Route de Narbonne, 31062 Toulouse, France.

<sup>[c]</sup> I. Physikalisches Institut, Universität zu Köln, Zùlpicher Str. 77, 50937 Köln, Germany.

<sup>[d]</sup> Radboud University, Institute for Molecules and Materials, FELIX Laboratory, Toernooiveld 7c, 6525 ED, Nijmegen, The Netherlands.

\* christine.joblin@irap.omp.eu

# Contents

<b>1</b>	<b>Experimental</b>	<b>S-2</b>
1.1	Mass resolution of the experimental setup . . . . .	S-2
1.2	Ion production . . . . .	S-2
1.3	Isomer composition – chemistry . . . . .	S-3
<b>2</b>	<b>Calculations</b>	<b>S-4</b>
2.1	Molecular structure (energetics) . . . . .	S-5
2.2	Molecular structure of the bare ions . . . . .	S-5
2.3	Molecular structure of the ion-Ne complex . . . . .	S-5
2.4	Comparison of different methods . . . . .	S-7
2.5	Influence of the Ne tag . . . . .	S-8
2.6	Influence of the Ne tag for $\text{Tr}^+$ . . . . .	S-10
2.7	Influence of the Ne tag for $\text{Bz}^+$ . . . . .	S-12
2.8	Combination band of $\text{Tr}^+$ . . . . .	S-13
2.9	Excited electronic state of $\text{Tr}^+$ . . . . .	S-13
<b>3</b>	<b>Visualisation of vibrational modes</b>	<b>S-14</b>

# 1 Experimental

## 1.1 Mass resolution of the experimental setup

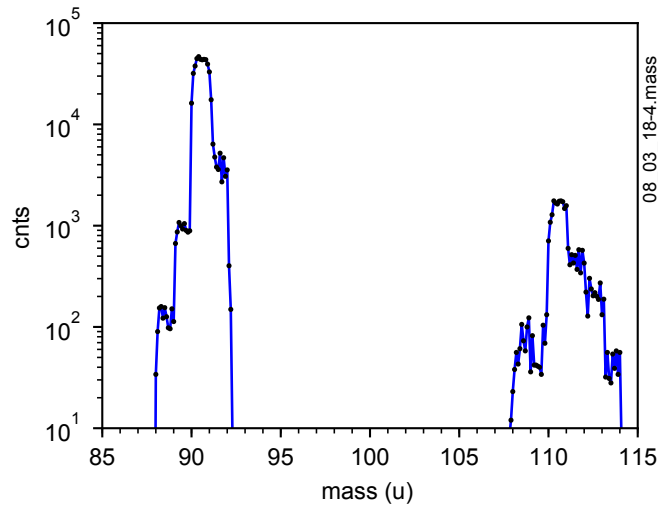


Figure S1: Mass resolution of the experimental setup. Ions of interest ( $\text{C}_7\text{H}_7^+$ , 91  $u$ ) are mass selected in the source quadrupole and injected into the trap. At the same time, a buffer gas pulse (He:Ne mixture cca. 3:1, pulse length 100 ms) is applied in order to aid thermalisation and promote ternary attachment. The ionic products are extracted after 500 ms storage time and mass selected in the product quadrupole (abscissa). Nominal trap temperature is 9 K. We achieved up to 5 % Ne attachment.

## 1.2 Ion production

Table S1: Precursors and source conditions used for ion production. Chemical probing (cf. Section 1.3) is used to obtain the abundance of benzylium.

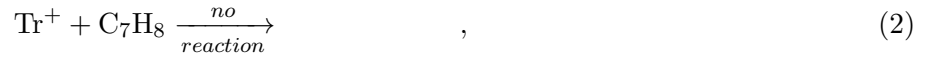
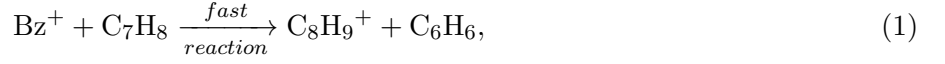
Precursor	Benzyl chloride $\text{C}_7\text{H}_7\text{Cl}$	Toluene $\text{C}_7\text{H}_8$	Toluene $\text{C}_7\text{H}_8$
Electron energy (approx.) (eV)	25	11*	25
Benzylium <sup>+</sup> (%)	> 90	~ 30	$\gtrsim$ 60

**Note:** Ions are produced in the storage ion source. They are extracted in a pulse shorter than 1 ms, after residence exceeding tens of ms. The amount of  $\text{Bz}^+$  we report in this table, is not strictly the electron bombardment yield, but rather the product of ion-molecule reactions inside the source.

\*– lowest electron energy for reasonable ion yield.

### 1.3 Isomer composition – chemistry

The reaction of  $C_7H_7^+$  with toluene



is used to determine the fraction of  $Bz^+$  in the mixture. Time evolution of reactants and products in the trap is shown in Fig. S2.

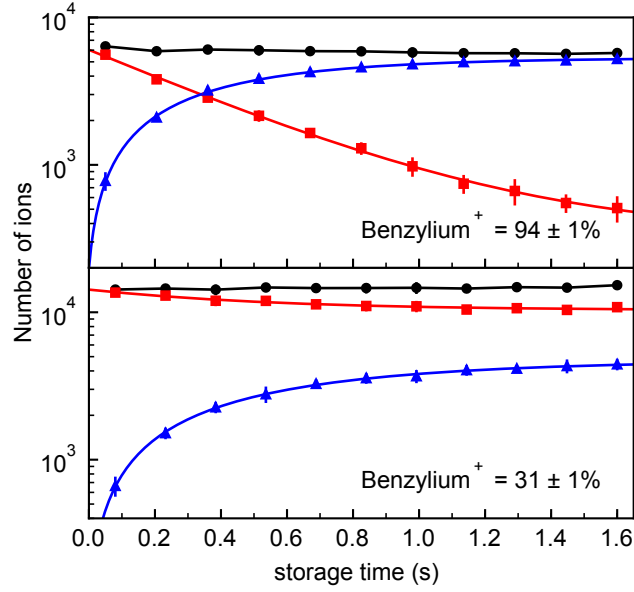


Figure S2: Number of ions in the trap as a function of the storage time. Red –  $C_7H_7^+$  (91  $u$ ). Blue –  $C_8H_9^+$  (105  $u$ ). Black – sum of all ions. Full lines represent exponential increase/ decay fits. The ratio between the reactive and non-reactive component of  $C_7H_7^+$  is calculated from the fitted parameters. We show the best conditions achieved for  $Bz^+$  isomer (upper panel) and  $Tr^+$  isomer (lower panel).

Note: Ions are trapped using a He pulse (tens of ms) at the beginning of the cycle. Neutral reactant, toluene, is leaked into the trap continuously mixed with He carrier gas ( $\sim 3.5\%$ ) and its estimated number density is  $8 \cdot 10^8 \text{ cm}^{-3}$ . Nominal trap temperature is 240 – 250 K.

## 2 Calculations

All calculations were performed in Gaussian09. They were computed in the  $C_{2v}$  symmetry point group. The following methods and basis sets were used:

- B3LYP/6-31G(d,p)
- B3LYP/cc-pvdz
- B3LYP/cc-pvtz
- wB97XD/cc-pvdz
- wB97XD/cc-pvtz
- MP2/cc-pvtz
- B2PLYP/cc-pvtz

Molecules  $Bz^+$ ,  $Bz^+ \cdot Ne(T, S)$ ,  $Tr^+ \cdot Ne(S)$  belong to  $C_{2v}$  point group. Molecules  $Tr^+$  and  $Tr^+ \cdot Ne(T)$  belong to  $D_{7h}$  point group. The descent in symmetry from  $D_{7h}$  point group to  $C_{2v}$  point group is presented in Tab. S2.

Table S2: The descent in symmetry from  $D_{7h}$  to  $C_{2v}$  for the  $Tr^+$  ion (experimentally observed bands only). Calculated values ( $\nu$ , Inten.) correspond to the B3LYP/6-31G(d,p) level of theory.

Mode	Exp.		Calc.		
	$\nu$ ( $cm^{-1}$ )	$\nu$ ( $cm^{-1}$ )	Inten. ( $km \cdot mol^{-1}$ )	Sym. $D_{7h}$	Sym. $C_{2v}$
$\nu_c$	630				
$\nu_4$	652	646	85.8	$A''_2$	$B_2$
$\nu_8$	994	989	3.7	$E'_1$	$A_1 + B_1(*)$
$\nu_{14}$	1486	1480	42.9	$E'_1$	$A_1 + B_1(*)$

Note: (\*)– Split degeneracies. Scaling factor 0.974.

## 2.1 Molecular structure (energetics)

Table S3: Relative energies (including zero point energy corrections) of  $\text{Tr}^+$  vs.  $\text{Bz}^+$  (black) and  $\text{Tr}^+ \cdot \text{Ne}$  (T) vs. (P) (red) and  $\text{Bz}^+ \cdot \text{Ne}$  (T) vs. (P) (blue) using the different theoretical methods.

$\Delta(\text{E} + \text{ZPE}) (\text{kJ} \cdot \text{mol}^{-1})$	$\text{Bz}^+$	$\text{Tr}^+$	$\text{Bz}^+ \cdot \text{Ne}$ (T)	$\text{Bz}^+ \cdot \text{Ne}$ (P)	$\text{Tr}^+ \cdot \text{Ne}$ (T)	$\text{Tr}^+ \cdot \text{Ne}$ (P)
B3LYP/6-31G(d,p)	+38	0	+8.6	0	+7.1	0
B3LYP/cc-pvtz	+36	0	+1.9	0	+1.5	0
wB97XD/cc-pvdz	+36	0	+5.7	0	+5.0	0
wB97XD/cc-pvtz	+34	0	+0.4	0	0	+0.65
MP2/cc-pvtz	+42	0	+0.2	0	+0.07	0
B2PLYP/cc-pvtz	+31	0	+1.5	0	+1.2	0

*Note:* The wB97XD/cc-pvtz and MP2/cc-pvtz levels of theory are expected to be the best approaches used to describe the systems studied in this work (wB97XD takes into account dispersion and long range interactions, MP2 is post Hartree Fock, using large cc-pvtz basis set).

## 2.2 Molecular structure of the bare ions

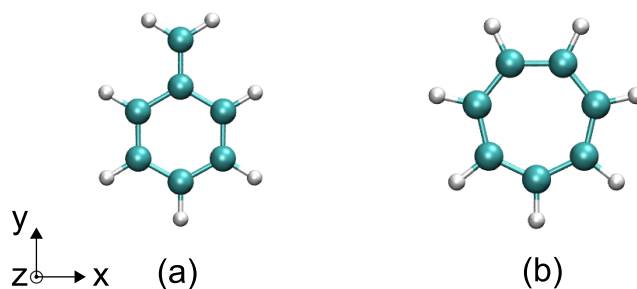


Figure S3: Structure of  $\text{Bz}^+$  (a) and  $\text{Tr}^+$  (b). The  $\text{Tr}^+$  structure is energetically more favorable (Tab. S3).

## 2.3 Molecular structure of the ion-Ne complex

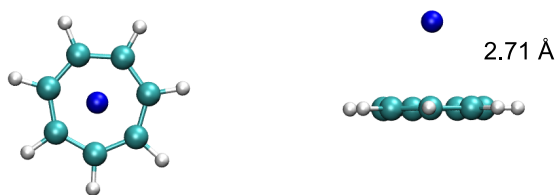


Figure S4: Structure of  $\text{Tr}^+ \cdot \text{Ne}(\text{T})$  with Ne on top of the molecular plane. This structure and the structure with Ne in the molecular plane (Fig. S5) are quasi degenerate (Tab. S3, especially at the wB97XD/cc-pvtz and MP2/cc-pvtz levels of theory).



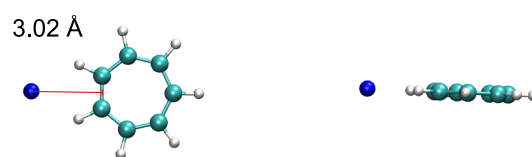


Figure S5: Structure of  $\text{Tr}^+ \cdot \text{Ne(P)}$  with Ne in plane with the molecule.

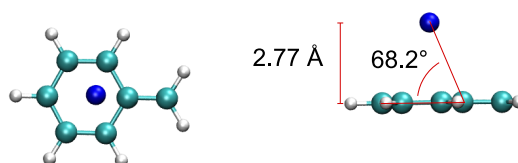


Figure S6: Structure of  $\text{Bz}^+ \cdot \text{Ne(T)}$  with Ne on top of the molecular plane. Calculated relative energies at the wB97XD/cc-pvtz and MP2/cc-pvtz levels of theory (Tab. S3) are well below  $1 \text{ kJ} \cdot \text{mol}^{-1}$  for all the structures in Figs. S6 – S8, thus, we consider these as quasi degenerate.

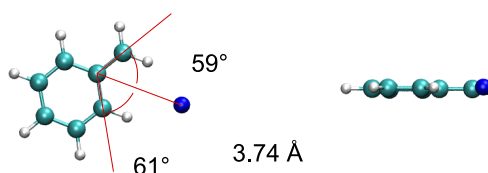


Figure S7: Structure of  $\text{Bz}^+ \cdot \text{Ne(P)}$  with Ne in plane with the molecule (Ne next to  $\text{CH}_2$ ). Note that according to the calculations (Tab. S3), this is the  $\text{Bz}^+ \cdot \text{Ne}$  structure with the lowest energy.

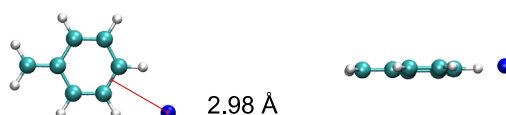


Figure S8: Structure of  $\text{Bz}^+ \cdot \text{Ne}$  with Ne in plane with the molecule. (Ne opposite to  $\text{CH}_2$ ).

## 2.4 Comparison of different methods

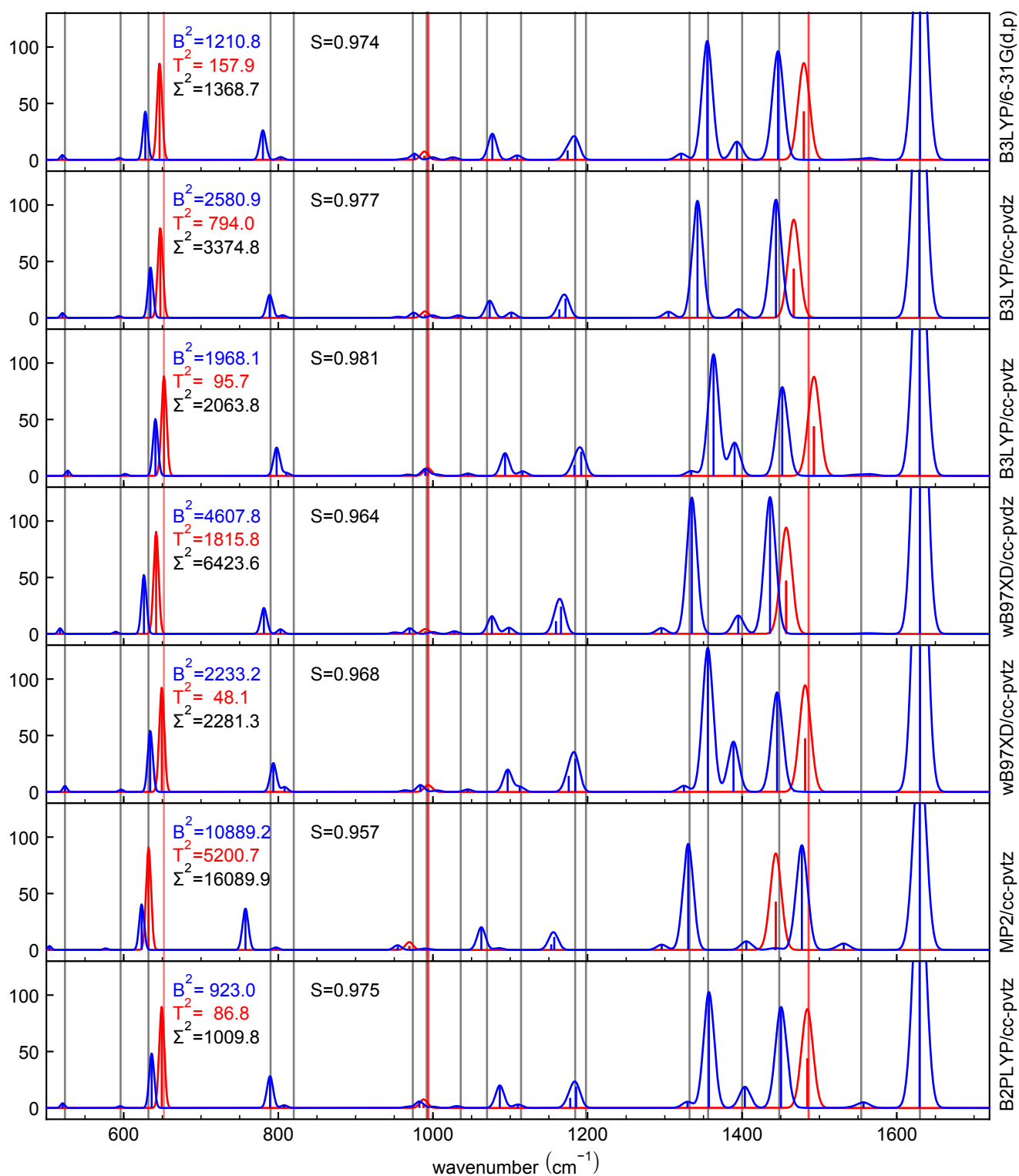


Figure S9: Comparison of the calculated spectra of  $Bz^+$  and  $Tr^+$ , obtained by the different methods with experimental data.  $B^2$ ,  $T^2$ ,  $\Sigma^2$  represent the sum of squares of “calculated – measured” positions for  $Bz^+$ ,  $Tr^+$ , and their sum, respectively. Only bands marked with vertical lines (experimental data, Tab. 1 and Tab. 2 in the text) are used in the calculations.  $S$  corresponds to the scaling factor determined using the  $1630\text{ cm}^{-1}$  band of  $Bz^+$ .

## 2.5 Influence of the Ne tag

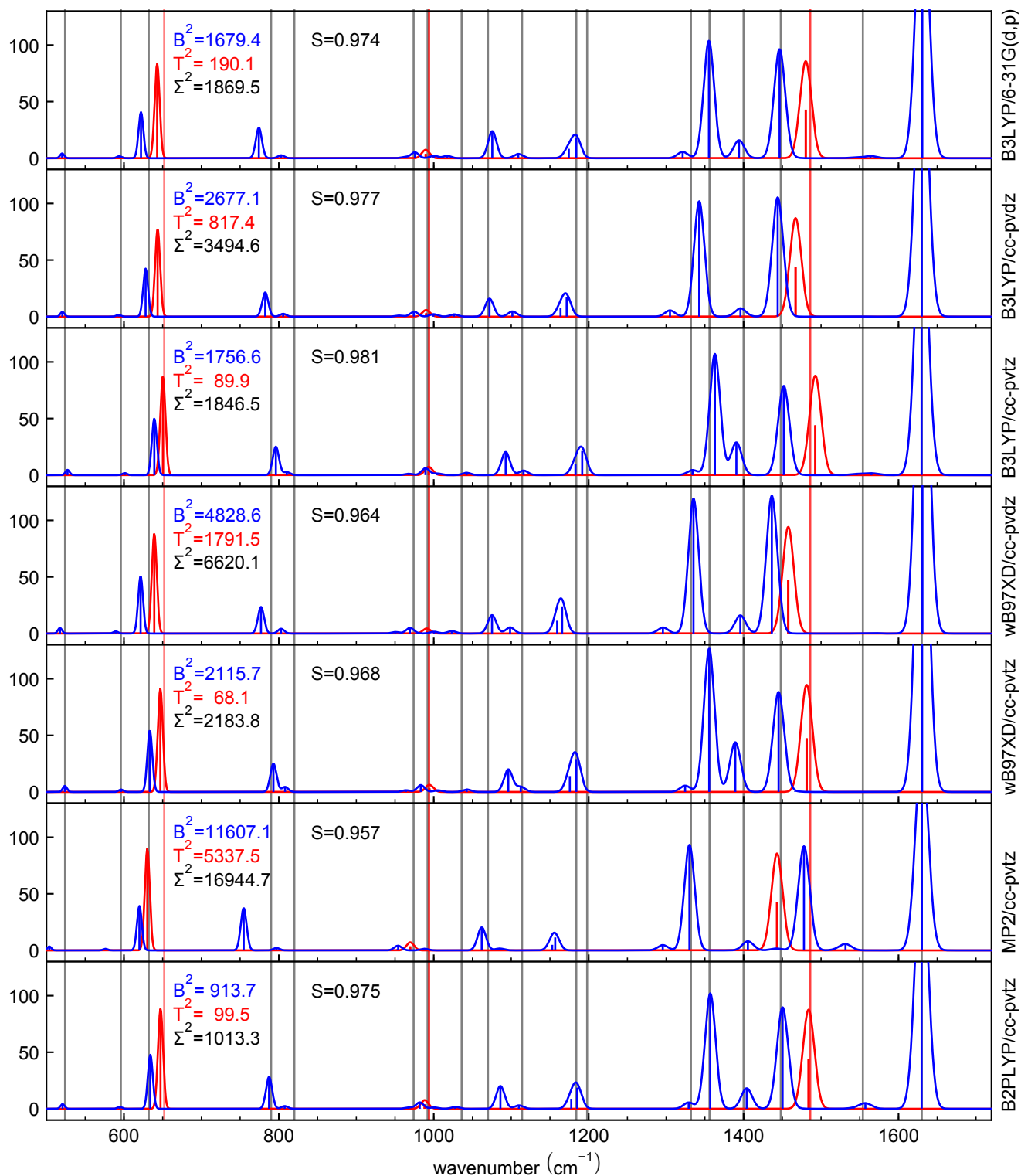


Figure S10: Comparison of the calculated spectra of  $Bz^+ \cdot Ne$  and  $Tr^+ \cdot Ne$ , obtained by the different methods with experimental data. Ne attached on top of the molecular plane (cf. Figs. S4, S6).  $B^2$ ,  $T^2$ ,  $\Sigma^2$  represent the sum of squares of “calculated – measured” positions for  $Bz^+ \cdot Ne$ ,  $Tr^+ \cdot Ne$ , and their sum, respectively. Only bands marked with vertical lines (experimental data, Tab. 1 and Tab. 2 in the text) are used in the calculations.  $S$  corresponds to the scaling factor (determined using the  $1630 \text{ cm}^{-1}$  band of  $Bz^+$ , cf. Fig. S9).

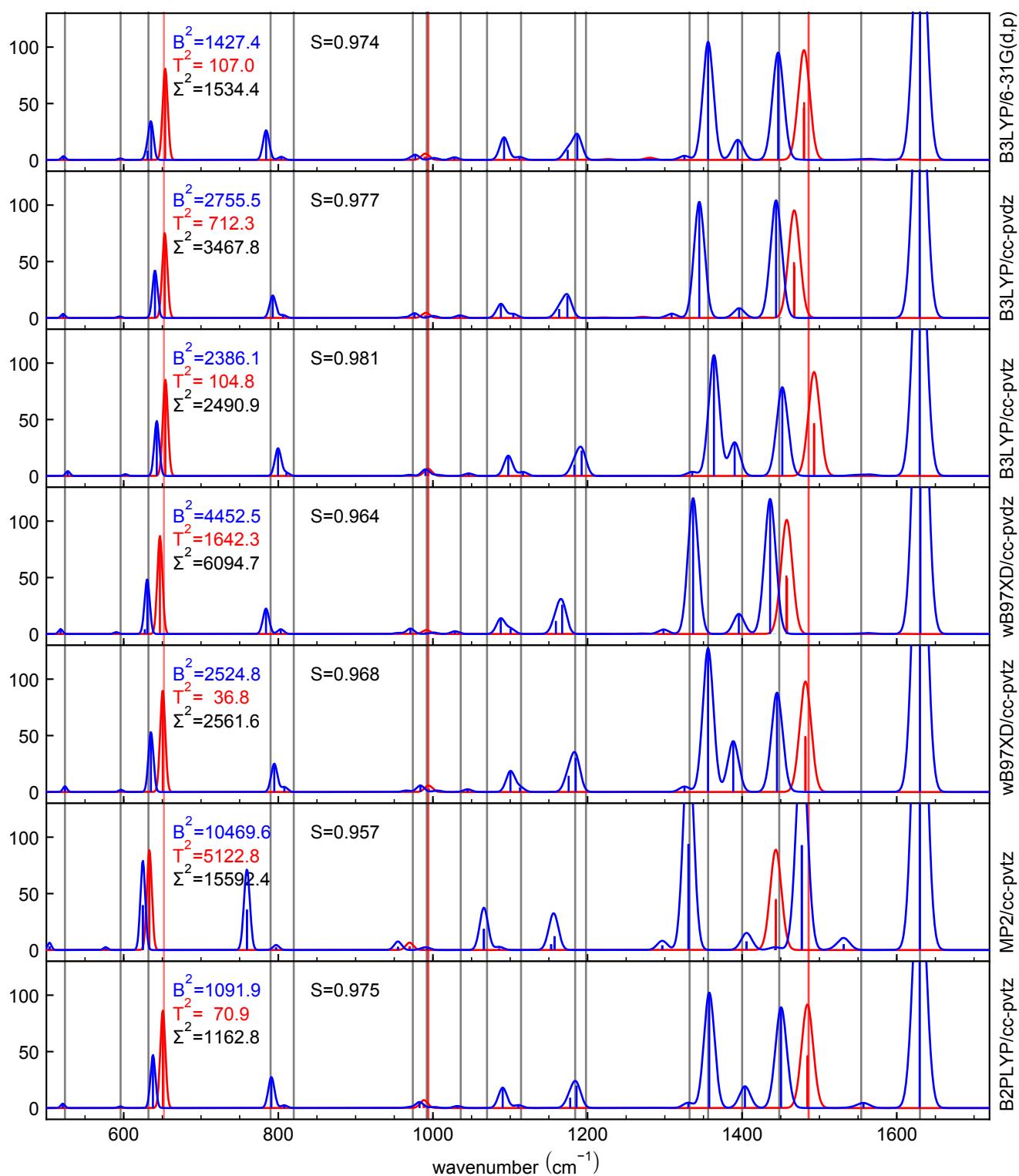


Figure S11: Comparison of the calculated spectra of  $Bz^+ \cdot Ne$  and  $Tr^+ \cdot Ne$ , obtained by the different methods with experimental data. Ne attached in the molecular plane (cf. Figs. S5, S7).  $B^2$ ,  $T^2$ ,  $\Sigma^2$  represent the sum of squares of “calculated – measured” positions for  $Bz^+ \cdot Ne$ ,  $Tr^+ \cdot Ne$ , and their sum, respectively. Only bands marked with vertical lines (experimental data, Tab. 1 and Tab. 2 in the text) are used in the calculations.  $S$  corresponds to the scaling factor (determined using the  $1630 \text{ cm}^{-1}$  band of  $Bz^+$ , cf. Fig. S9).

## 2.6 Influence of the Ne tag for $\text{Tr}^+$

Table S4: Shift of the  $\text{Tr}^+$  band around  $650\text{ cm}^{-1}$  as a function of the  $\text{Tr}^+ \cdot \text{Ne}$  configuration for different calculation methods. The shift predicted by the best levels of theory used to describe the systems studied in this work (wB97XD/cc-pvtz and MP2/cc-pvtz) is just below the resolution of our experiment.

Method	$\text{Tr}^+$	+Ne (top)	+Ne (plane)	$\Delta$ Ne (plane – top)
B3LYP/6-31G(d,p)	663.6	660.0	671.2	11.2
B3LYP/cc-pvtz	664.8	662.9	666.6	3.7
wB97XD/cc-pvdz	665.9	663.1	671.0	7.9
wB97XD/cc-pvtz	648.6	646.3	649.8	3.5
MP2/cc-pvtz	660.6	658.5	661.6	3.1
B2PLYP/cc-pvtz	665.8	663.8	667.3	3.5

**Note:** All frequencies in  $\text{cm}^{-1}$ . Frequencies are not scaled. In Ne IR-PD experiment, the distance between the two observed bands is  $22\text{ cm}^{-1}$ .

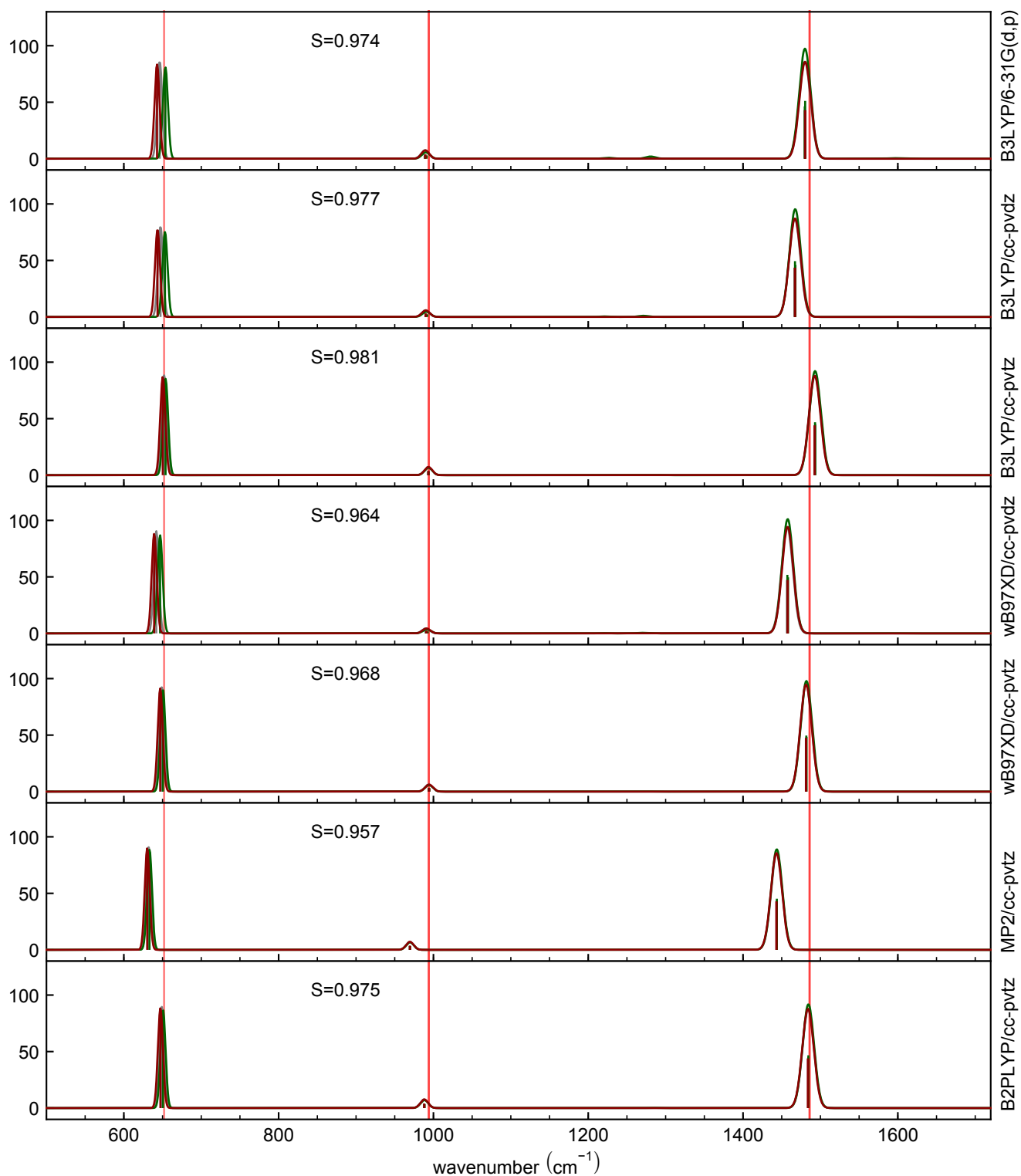


Figure S12: Spectra corresponding to different positions of the Ne atom attached to  $\text{Tr}^+$ . S corresponds to the scaling factor (determined using the  $1630\text{ cm}^{-1}$  band of  $\text{Bz}^+$ , cf. Fig. S9). Color code: grey – bare ion, dark red – Ne on top of the molecular plane (cf. Figs. S4), dark green – Ne in the molecular plane (cf. Figs. S5).

## 2.7 Influence of the Ne tag for Bz<sup>+</sup>

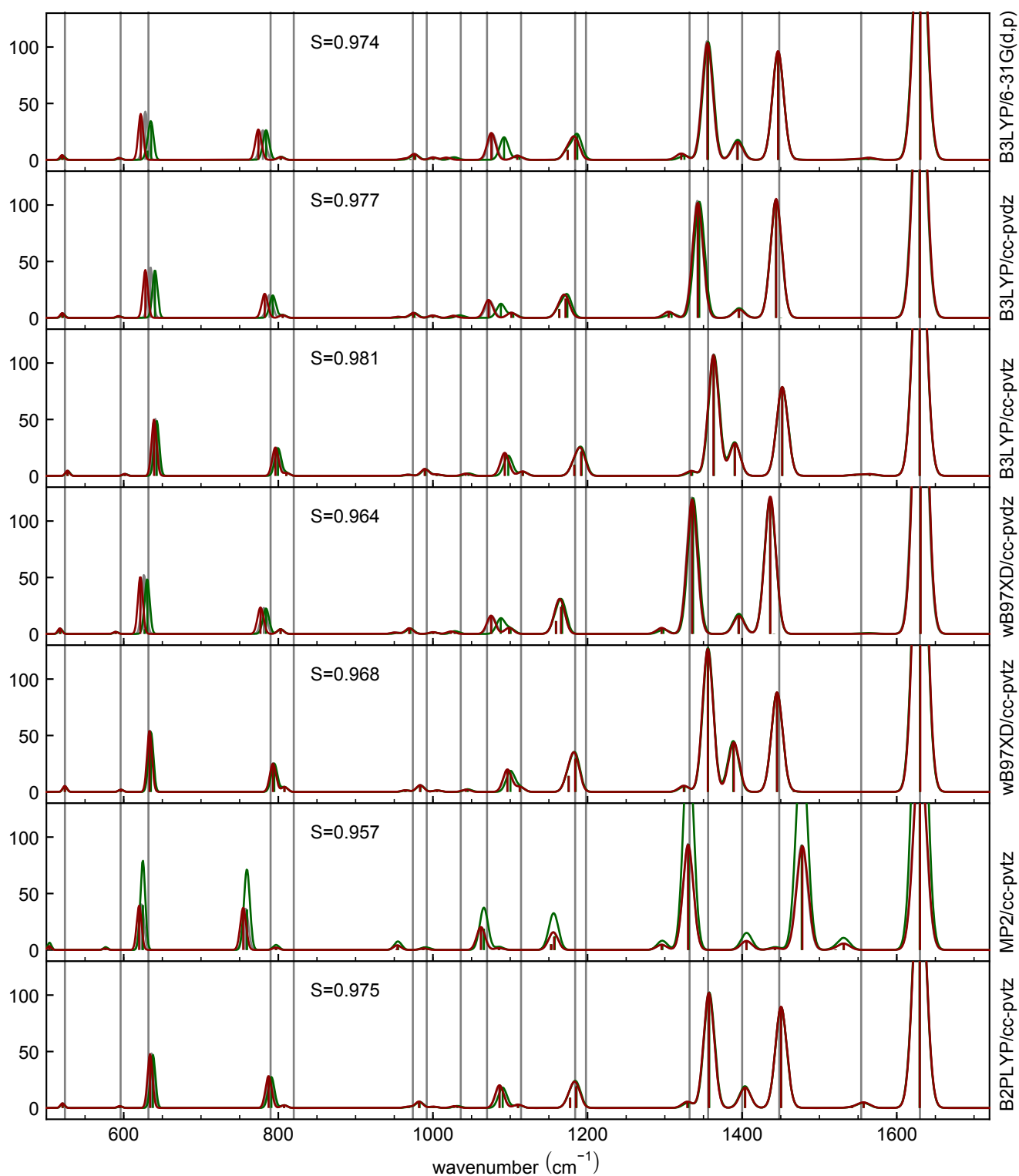


Figure S13: Spectra corresponding to different positions of the Ne atom attached to Bz<sup>+</sup>. S corresponds to the scaling factor (determined using the 1630 cm<sup>-1</sup> band of Bz<sup>+</sup>, cf. Fig. S9). Color code: grey – bare ion, dark red – Ne on top of the molecular plane (cf. Figs. S6), dark green – Ne in the molecular plane (cf. Figs. S7).



## 2.8 Combination band of $\text{Tr}^+$

Table S5: Comparison of position of the  $\text{Tr}^+$  and  $\text{Tr}^+ \cdot \text{Ne}$  out of plane CH bend around  $650 \text{ cm}^{-1}$  with possible combination bands.

	B3LYP/6-31G(d,p)			wB97XD/cc-pvtz			MP2/cc-pvtz		
	$\text{Tr}^+$	$\text{+Ne (T)}$	$\text{+Ne (P)}$	$\text{Tr}^+$	$\text{+Ne (T)}$	$\text{+Ne (P)}$	$\text{Tr}^+$	$\text{+Ne (T)}$	$\text{+Ne (P)}$
$\omega_{\text{Ne } 0}$		42.3	40.3		20.6	19.6		28.4	15.6
$\omega_{\text{Ne } 1}$		42.7	59.2		26.5	27.6		28.4	30.9
$\omega_{\text{Ne } 2}$		96.0	106.7		42.3	50.4		56.7	47.8
$\omega_0$	218.4	211.6	220.1	213.5	211.0	213.8	206.0	203.6	206.4
$\omega_1$	218.9	212.3	224.9	213.7	212.4	214.9	206.0	203.6	207.5
$\omega_2$	427.2	427.1	428.2	426.7	426.2	427.2	407.8	407.2	407.9
$\omega_3$	427.7	427.7	428.2	427.1	426.7	427.4	407.8	407.2	408.1
$\omega_4$	549.4	541.2	551.7	552.1	549.7	552.7	531.0	528.1	531.9
$\omega_5$	549.6	541.6	552.7	552.3	550.0	553.1	531.0	528.1	532.2
$\omega_6$	646.4	642.9	653.7	649.3	647.0	650.5	632.2	630.2	633.2
$\omega_{\text{Ne } 2} + \omega_4$		637.2	658.3		591.9	603.1		584.8	579.7
$\omega_0 + \omega_2$	645.6	638.7	648.3	640.1	637.1	641.0	613.9	610.8	614.3

**Note:** All frequencies in  $\text{cm}^{-1}$ . All modes except  $\omega_6$  ( $I \sim 80 \text{ km} \cdot \text{mol}^{-1}$ ) and  $\omega_{\text{Ne } 2}$  ( $I \sim 3 \text{ km} \cdot \text{mol}^{-1}$ ) have zero intensities. (T) – Ne on the of the molecular plane, (P) – Ne in the molecular plane.

## 2.9 Excited electronic state of $\text{Tr}^+$

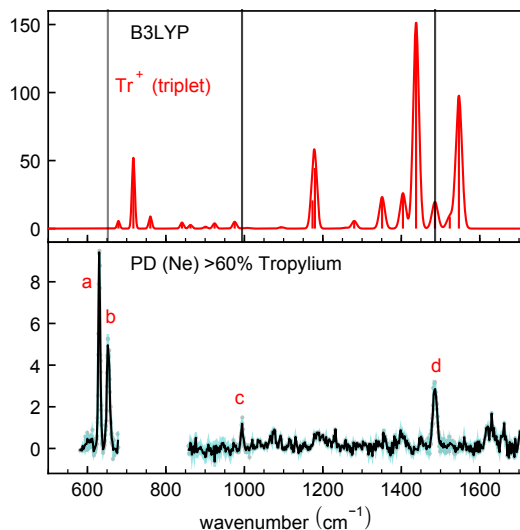


Figure S14: Calculated frequencies of the triplet state of  $\text{Tr}^+$  at the B3LYP/6-31G(d,p) level of theory (scaling factor 0.974) compared to the Ne IR-PD spectrum of  $\text{Tr}^+$ .

### 3 Visualisation of vibrational modes

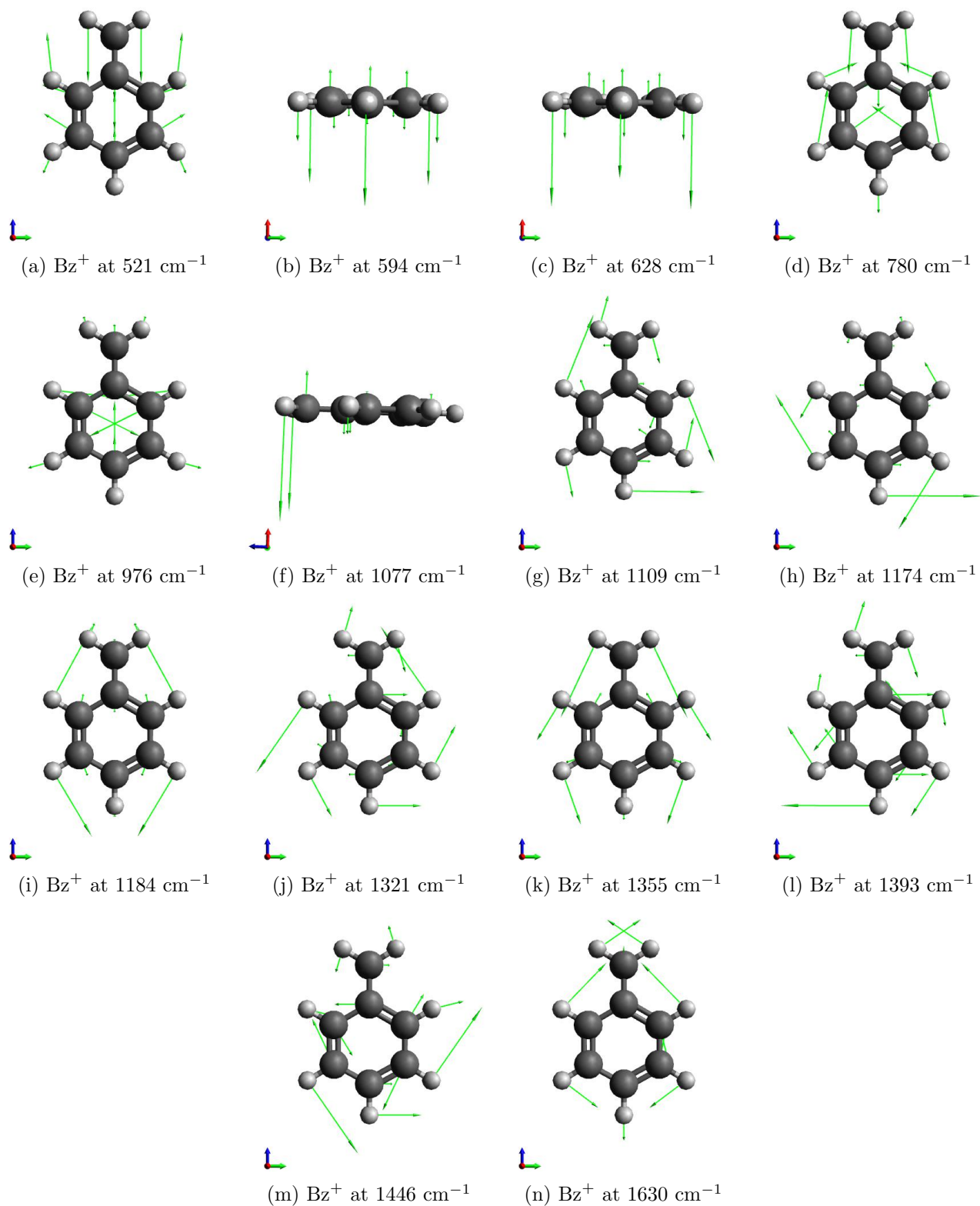
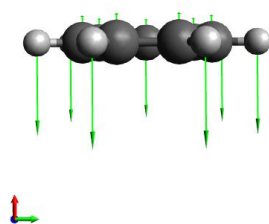
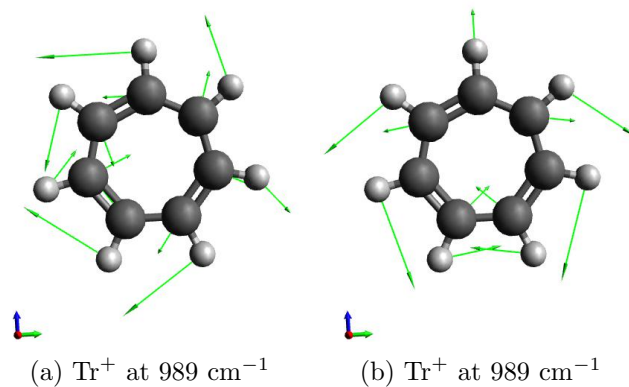


Figure S15: Harmonic vibrational modes of  $\text{Bz}^+$  calculated at the B3LYP/6-31G(d,p) level of theory, scaling factor 0.974.



(a)  $\text{Tr}^+$  at  $646\text{ cm}^{-1}$

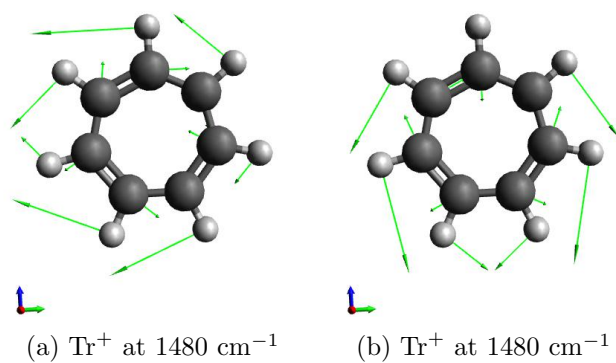
Figure S16: Harmonic vibrational modes of  $\text{Tr}^+$  calculated at the B3LYP/6-31G(d,p) level of theory, scaling factor 0.974. Out of plane CH bending.



(a)  $\text{Tr}^+$  at  $989\text{ cm}^{-1}$

(b)  $\text{Tr}^+$  at  $989\text{ cm}^{-1}$

Figure S17: Harmonic vibrational modes of  $\text{Tr}^+$  calculated at the B3LYP/6-31G(d,p) level of theory, scaling factor 0.974. In plane CH bending mode.



(a)  $\text{Tr}^+$  at  $1480\text{ cm}^{-1}$

(b)  $\text{Tr}^+$  at  $1480\text{ cm}^{-1}$

Figure S18: Harmonic vibrational modes of  $\text{Tr}^+$  calculated at the B3LYP/6-31G(d,p) level of theory, scaling factor 0.974. In plane CC stretching mode.